Unveiling hidden risks in healthcare from flood-induced transportation disruption in Germany

Wassmer, Jonas; Bryant, Seth; Schimansky, Paul; Keegan, Lindsay T.; Pregnolato, Maria; Kurths, Jürgen; Marwan, Norbert; Merz, Bruno

DOI
10.1038/s43247-025-02645-y

Publication date
2025

Document Version
Final published version

Published in
Communications Earth and Environment

communications earth & environment

Article

A Nature Portfolio journal

https://doi.org/10.1038/s43247-025-02645-y

Unveiling hidden risks in healthcare from flood-induced transportation disruption in Germany

Jonas Wassmer[1,2,8], Seth Bryant[1,3,8] ✉, Paul Schimansky[1], Lindsay T. Keegan[4], Maria Pregnolato[5,6], Jürgen Kurths[2], Norbert Marwan[2,7,9] & Bruno Merz[1,3,9]

Despite investments in disaster resilience, flooding continues to disrupt healthcare systems, both by limiting access and through failures in the surrounding transportation network. Existing models for mitigation planning often overlook critical dynamics, such as traffic rerouting, particularly at the national scales necessary for effective planning. Here we present a scalable method to identify hospitals at risk of emergency response delays and service disruptions caused by flood-induced traffic impacts. Our approach integrates a regional flood model with a gravity-based traffic model to simulate traffic flow from open-source road data. Our findings reveal hidden risks for hospitals located far from flood zones, showing how flood-related road disruptions and traffic rerouting can reduce access to critical healthcare services. In particular, we found 75 (of 2,475) hospitals at risk of patient surges beyond their regular capacity, driven solely by flood-related traffic disruptions. Of these, a third are more than 10 km from the nearest inundation, suggesting these facilities may be unaware and thus under-prepared — risks that have, until now, remained hidden from assessments.

Natural hazards such as fluvial flooding[1–3] and hurricanes[4–6] have had profound impacts on healthcare systems with widespread human, economic, and political consequences[7,8]. These disasters can lead to overcrowded hospitals, causing increased morbidity and mortality[9–12] and can trigger secondary crises, such as the spread of infectious diseases or deterioration of chronic conditions[13,14]. Even brief interruptions in access to care can adversely affect patient outcomes[15], while prolonged disruptions can undermine public trust and destabilize communities[16,17]. Building resilient healthcare systems capable of withstanding such crises requires effective disaster planning, coordination, and training, which require accurate and robust information[18–20]. Additionally, the increasing frequency and intensity of extreme weather events driven by climate change underscore the urgent need for more resilient healthcare infrastructure[21].

A key component of healthcare system resilience is a robust transportation network, which is critical for ensuring the timely movement of patients and medical resources[15,22]. However, these networks are widely exposed to flooding[23] and particularly vulnerable because a small number of road segments account for most hospital access[24,25]. As a result, flood-induced road damage can cause widespread supply chain disruptions, delayed medical evacuations, and overwhelm hospitals with patients[26], as happened in the 2011 floods in Thailand[2] and the 2023 floods in Italy[3]. When hospitals are forced to close due to flooding, the reconfiguration of service areas and increased patient load on neighboring facilities compounds the problem[3,6,27]. For example, severe flooding in 2021 led to the closure of St.-Antonius Hospital in Eschweiler, Germany, resulting in the transfer of patients to seven neighboring facilities[28], overburdening them amid disrupted road networks and higher travel times (see Supplementary Table 1 and Supplementary Note 1 for an extended discussion of this event). Understanding these vulnerabilities in the healthcare-transport system, and the ways in which flood-induced disruptions amplify them, is the central focus of our study.

Flooding can lead to both direct damage to infrastructure like roads and bridges[29,30], as well as indirect impacts like prolonged congestion due to traffic rerouting[31,32]. In some cases, these rerouting effects can induce congestion and increase travel times far beyond the apparent spatial and temporal boundaries of the inundation[33]. For example, the destruction of

[1]Institute of Environmental Science and Geography, University of Potsdam, Potsdam, Germany. [2]Potsdam Institute for Climate Impact Research (PIK), Member of the Leibniz Association, Potsdam, Germany. [3]GFZ German Research Center for Geosciences, Section 4.4. Hydrology, Potsdam, Germany. [4]Division of Epidemiology, Department of Internal Medicine, University of Utah, Salt Lake City, UT, USA. [5]University of Bristol, Department of Civil Engineering, Bristol, UK. [6]Delft University of Technology, Department of Hydraulic Engineering, Delft, Netherlands. [7]Institute of Geosciences, University of Potsdam, Potsdam, Germany. [8]These authors contributed equally: Jonas Wassmer, Seth Bryant. [9]These authors jointly supervised this work: Norbert Marwan, Bruno Merz.
✉e-mail: bryant.seth@gmail.com

bridges during a 2009 flood in England led to an eight-fold increase in travel times that lasted for six months[34]. Even in cases with mild infrastructure damage, ambulance response times can double[35]. Such delays are not without consequence. Comparable traffic disruptions, such as those observed during city-wide marathons in the United States, have been linked to a 13% increase in mortality[15] and have been shown to deteriorate the quality of care, contributing to increases in morbidity and mortality in many regions[10,36–38].

To predict and study travel patterns, traffic models formalize assumptions about vehicle flow and movement dynamics. These models are typically categorized as microscopic, mesoscopic, or macroscopic depending on the level of detail and scale considered. Microscopic models, such as agent-based simulations, model individual vehicle and driver interactions, enabling them to capture complex phenomena like congestion, queuing, and lane-changing behavior[39,40]. While these models have been successfully applied to large-scale urban scenarios—such as simulating traffic in Berlin[41]—they are computationally intensive and generally impractical for analyzing user equilibrium traffic or system-wide rerouting on larger, national-scale networks[42,43]. Mesoscopic models on the other hand, balance detail between the high-resolution of microscopic models and the computational efficiency of macroscopic ones. They simulate individual vehicles but rely on aggregate flow representations, often using speed-density relationships and queuing theory to approximate congestion dynamics[44]. While they are more scalable than microscopic models, their reliance on parameter calibration and simplified behaviors limits their applicability for large-area planning or assessment. Macroscopic models, in contrast, treat traffic as a continuous flow, focusing on aggregate quantities like vehicle density, speed, and flow rate[45]. Their scalability makes them well-suited for national-scale applications. For example, the widely used *routing-based* macroscopic framework simplifies traffic patterns to a binary "disrupted or not" status, offering computational efficiency but limiting the framework's ability to capture real-world congestion from rerouting during major disruptive events[46,47]. Other approaches include *shortest path analyses*[48] and solving for a user equilibrium in a Traffic Assignment Problem (TAP)[49], where each driver chooses the route that minimizes their individual travel time based on network-wide congestion. However, solving TAPs becomes computationally demanding as network size increases, especially when iteratively updating travel costs based on congestion. To address this tradeoff between realism and scalability, a promising alternative is the gravity-based macroscopic model, which serves as a conceptual bridge between shortest-path models and TAPs. This method assumes that travel occurs proportionally between origin-destination pairs based on their "mass" (e.g., population), similar to Newtonian gravity, and assigns traffic using fixed, free-flow travel times[50]. Such gravity-based models can be considered a special case of TAP—sometimes referred to as the shortest path limit—in which drivers do not respond to congestion during routing, but delays are estimated afterwards using nonlinear cost functions[51]. Gravity-based models have been useful in other fields, such as economics[52], migration[53], and urban communication networks[54]. These models are scalable and computationally efficient, making them a promising framework for traffic modeling at scale.

Traffic behaviors are especially relevant to understand the dependence of healthcare systems on transportation networks[55]. In a landmark study on such healthcare-transportation systems under flooding, Yu et al.[46] quantified the degradation in ambulance response times for England (UK) driven by three flood event return periods using 50 m resolution flood maps. To compute response times at this scale, Yu et al.[46] employed two key simplifications. First, risk- rather than simulation-based flood maps were used, leading to implausible flood footprints at large spatial-scales[56]. Second, their routing-based analysis did not consider congestion caused by rerouting around disrupted road segments[57], which is a major driver of travel times[47,58]. To capture such dynamics while maintaining computational feasibility, Wassmer et al.[33] developed a gravity-based traffic model parameterized by open-source data for a 2021 flood. This model represents road networks as directed graphs and simulates traffic flow by assuming the probability of travel between locations is weighted by population size and travel time. Their findings demonstrated the impact of flood-related traffic disruptions, showing for example that 20,000 people lost access to 15 min Emergency Medical Services—the maximum allowed by most federal states in Germany[59].

These previous studies have provided important insights and advanced methodologies for evaluating traffic-related health system vulnerability. However, they were either limited in scope—focusing on relatively small regions—or overly simple, omitting important mechanisms like rerouting. Our work addresses these shortcomings by employing a gravity-based method that is sufficiently sophisticated and scalable to capture the regional dynamics necessary for resilience planning. Expanding the traffic model of Wassmer et al.[33] to the national scale and joining it to a process-based flood model, we uncover critical vulnerabilities to the health sector and provide the understanding necessary to improve the disaster resilience of healthcare-transport systems. Furthermore, our method facilitates the production of interactive flood and traffic scenario maps which are needed by healthcare and transportation authorities for mitigation planning. This work demonstrates a generalizable method for assessing healthcare system resilience to floods and highlights the importance of considering traffic disruptions when planning—even for facilities where direct flooding is unlikely.

Results

Healthcare-transport system vulnerabilities

Figure 1 provides an overview of system-wide vulnerability by showing the maximum increase in service population found across all flood scenarios, expressed as $\max(N(k_H))$. This increase in service population, defined as the expected number of patients likely to access the facility (see Methods 6.5), estimates indirect flood-related patient surges to hospitals as a fraction of their baseline service population. This result shows a heterogeneous distribution of vulnerability extending far beyond the flood footprints included in our study. While some regions with low population densities or few major rivers are relatively insensitive to flood disruption, the results clearly show that healthcare-transport system vulnerability is a Germany-wide challenge. Focusing on the extremes, we find 75 hospitals with an increase in service population of more than 30% (Supplementary Table 3). Assuming that a temporary increase of 30% in population ($\Delta N(k_H)$ >0.3) would raise a hospital to full capacity[60], we interpret this result as roughly 75 unique hospitals being vulnerable to capacity exceedance as a result of flood-driven traffic disruptions. Even more alarming, 29 hospitals show an increase greater than 50%, while 9 increase more than 85% in service population (these nine are further discussed in the following section). To improve dissemination and help decision-makers identify specific vulnerabilities in their regions, interactive maps are provided in Supplementary Data 1 for the 75 facilities found to have a >30% increase in service population.

Comparing hazard frequency to traffic impacts shows that the vulnerability of any of our seven analysis basins (Fig. 1) is not strictly related to the number of flood events within our analysis set (see Supplementary Table 3 and Supplementary Table 2). For example, while the two basins with the fewest events (Ems and Upper Rhine) have minimal vulnerability (no hospitals with $\Delta N(k_H) \geq 0.3$), Lower Rhine, Upper Elbe, and Danube, which all have 36–38 flood events, differ substantially in vulnerable facility counts (132, 21, 118, respectively). This result demonstrates the non-linear relationship between flood hazards and healthcare-transport vulnerability and the importance of incorporating methods that can capture these non-linearities into risk assessments. Looking at the relative risks faced by each analysis basin, the Lower Rhine with its high population densities and history of extreme flooding unsurprisingly has the most vulnerable hospitals by count (for all $\Delta N(k_H)$ thresholds considered; see Supplementary Table 3), especially the riverine cities of Cologne and Frankfurt (see Supplementary Fig. 1 for location).

While computational constraints preclude any probability quantification about these vulnerabilities, the results suggest some facilities may face disruptions more often than others. For example, six of the 2475 facilities experienced 10 or more capacity-exceeding events (using $\Delta N(k_H) \geq 0.3$ as a threshold; see Supplementary Discussion 3). These repeated exposures

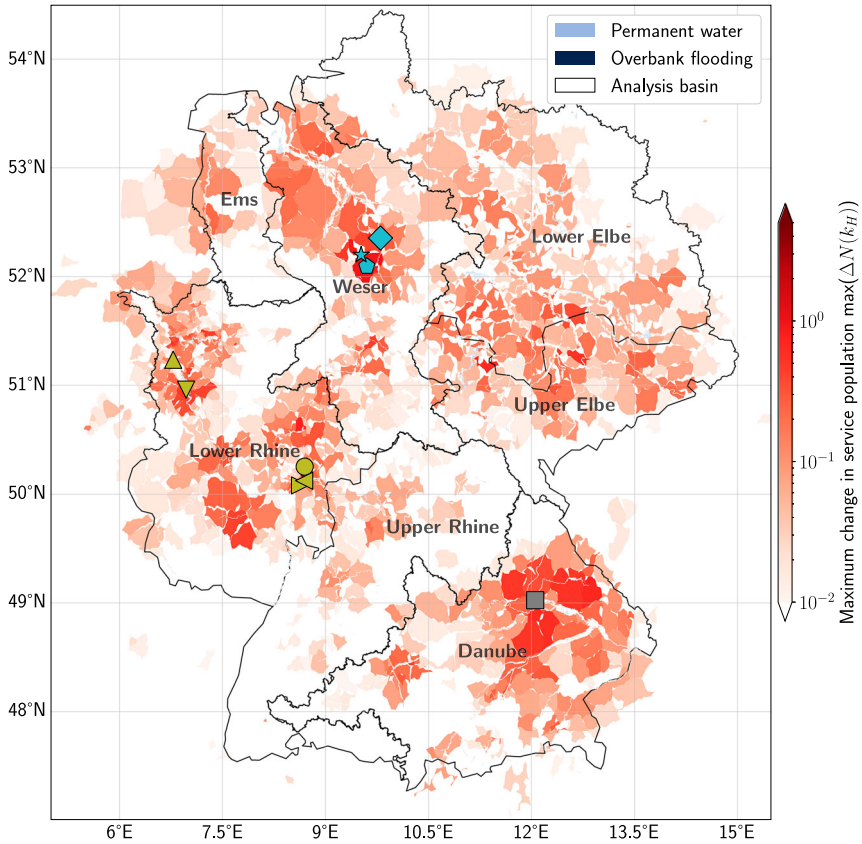

Fig. 1 | Flood-induced changes in hospital accessibility and service populations. The impact of simulated flood-induced road failures on hospital service areas shown as the maximum increase in service population (i.e., max($\Delta N(k_H)$); color gradient) and post-flood service regions (polygon area) for all analysis events. For clarity, hospitals with max($\Delta N(k_H)$) ≤ 10^{-2} are omitted. The nine symbols correspond to the hospitals shown in Figs. 2 and 3 and discussed further in the text. Also shown are the maximum overbank flooding, permanent water bodies, and analysis basins.

demonstrate that a minority of facilities face greater risk compared to their peers.

While our simulations focus mainly on flooding events within Germany, the results indicate that some hospitals outside of Germany also experience a major increase in service population. For example, 51 hospitals (18 in the Netherlands, 8 in Austria and Belgium, 7 in France, 5 in the Czech Republic, 3 in Luxembourg, and 1 in Poland and Switzerland) were found to have max($\Delta N(k_H)$) > 0.01. These findings highlight the challenges associated with cross-border disaster management, emphasizing the need for coordinated efforts and resource sharing between neighboring countries to effectively manage the increased demand on healthcare services after such disruptive events.

Considering the utility of quantifying healthcare-transport system vulnerability for emergency planning, of particular interest to our study are those hospitals far from flood inundation yet highly sensitive to indirect traffic impacts; what we call *hidden risk*. While a direct study of emergency plans is made difficult by their confidential nature, we assume that facilities far from flooding are less likely to consider flood-related impacts in their plans, making the identification of these risks particularly important for disaster resilience. To identify such facilities, Fig. 2 shows the change in service population vs. the distance to the nearest inundation w_{kl} for the maximum event for each hospital. The overall trend of this plot shows that hospitals closer to the flood yield larger increases in service population from flood-related traffic disruptions. In other words, the closer a facility is to flooding the more sensitive it is to traffic disruptions, usually. This situation is intuitive as traffic flow (and our model) is highly correlated in space, so we expect network effects to typically decay with distance. However, *not* all hospitals follow this trend. Consider the upper-right of Fig. 2 where both service population changes ($\Delta N(k_H)$) and distance from flooding (dist$_E(k_H, w_{kl})$) are large; here some facilities are found with both high vulnerability and a large distance from inundation (implying a lack of flood awareness). To better explore these hidden vulnerabilities, consider the aforementioned 75 hospitals at risk of capacity exceedance ($\Delta N(k_H)$ ≥0.3); of these, approximately one-third (26 facilities) are more than 10 km from the nearest inundation (see cross-hatch Fig. 2) while one-sixth (13 facilities) are more than 15 km (Supplementary Table 6). Of the facilities more than 10 km from the nearest inundation, two represent the most extreme cases overall with a near doubling of service population (discussed in the following section; Fig. 3f, g). Focusing on those furthest from the flood, we find two facilities at risk of capacity exceedance ($\Delta N(k_H)$ ≥0.3) yet over 30 km from the nearest inundation. This co-occurrence of high vulnerability and potential lack of awareness suggests a critical weakness in the healthcare system in Germany.

Highlighted vulnerabilities

To better understand the vulnerabilities considered by this study, Figure 3 presents nine scenarios extracted from our analysis representing the unique hospitals with the largest increase in service population ($\Delta N(k_H)$). Collectively, these scenarios demonstrate the potential for severe healthcare service disruption, with increases in service population ranging from 86% to 395%. All of these facilities fall within the Lower Rhine (5), Weser (3), or Danube (1) basins, which echos the above discussion on the level of risk in the Lower Rhine (see Supplementary Discussion 5 for extended discussion). Further, three of the nine $\Delta N(k_H)$ values are generated by a single event in Frankfurt (Lower Rhine #482). This event demonstrates a truly catastrophic scenario where numerous facilities and roads are disabled, directing patients to the few remaining hospitals. Although Germany has largely avoided a catastrophic major river flooding event like this in recent decades, the healthcare failures seen during Hurricane Harvey in Houston[47] offer an ominous precedent, highlighting the potential consequences of widespread disruptions to both facilities and infrastructure.

These nine scenarios demonstrate two important mechanisms. First, the loss of critical road links and the subsequent impact on travel times partially explain the effective service population increases in all nine scenarios. For example, panel (a) shows a scenario where the loss of roads and bridges across the River Main isolates the northern part of Frankfurt from

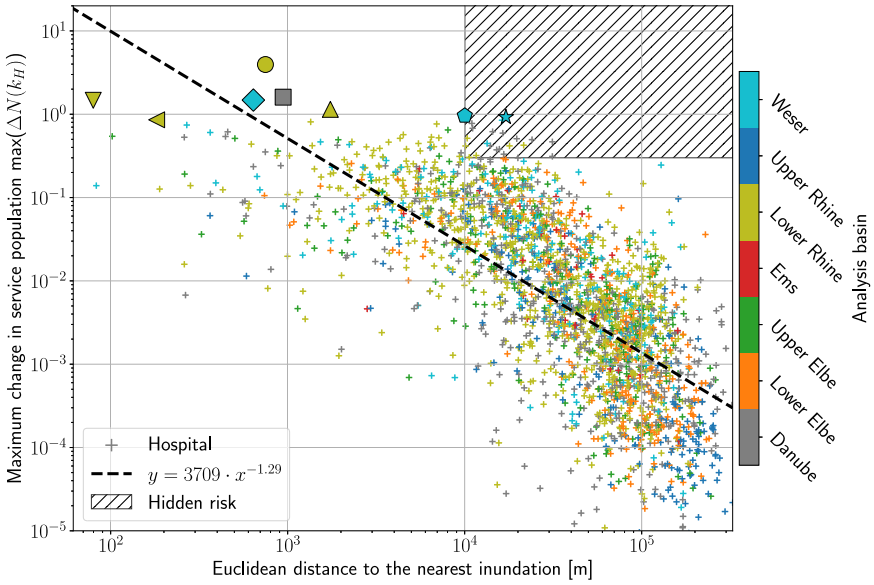

Fig. 2 | Hospital impacts and distance to flooding. Scatter plot for the maximum change in service population, $max(\Delta N(k_H))$, for all hospitals showing the Euclidean distance to the nearest point of inundation ($dist_E(k_H, w_{kl})$) and corresponding power law trend line (black dash; computed using linear least-squares regression) on a double logarithmic scale. Colors indicate the analysis basin. The large symbols show the nine facilities with the largest impacts as discussed in the text and Fig. 3. An example region of hidden risk is shown on the top right (cross-hatch) delineated by the $\Delta N(k_H) = 0.3$ threshold and $dist_E(k_H, w_{kl}) = 10$ km distance threshold.

the southern part. This isolation forces patients who previously would have crossed the river to now undertake a long drive to access healthcare at *Sankt Katharinen Krankenhaus*. Such disruptions can be long-lasting, similar to findings reported in England following a 2009 flood where destroyed bridges led to an eightfold increase in travel times that persisted for six months[34]. Second, the disabling of neighboring facilities and the subsequent redirection of patients to remaining facilities partially explain the $\Delta N(k_H)$ increase in all but one facility (panel c). For example, panel (d) shows a scenario where four hospitals in Cologne are disabled by floodwaters, leaving *Kinderkrankenhaus Amsterdamer Straße* to absorb the redirected patient load. A similar phenomenon was reported following the 2011 flooding in Thailand[2] and the 2023 flooding in Italy[3]. These scenarios highlight the link between regional transportation and facility capacity during crises and the need for holistic assessments in resilience planning. Such assessments should not be limited to facilities in flood zones, as highlighted by panels (f) and (g), which are 10 and 17 km from the nearest flooding respectively.

Discussion

This study presents a generalizable framework that joins a continuous-simulation high-resolution flood model with a gravity-based traffic model to assess healthcare system vulnerabilities in the face of flood-induced transportation disruptions. Our findings reveal critical risks to hospitals, not just from direct flood impacts, but also from indirect effects like traffic congestion and rerouting, which can severely delay emergency services and increase patient loads at facilities well outside the flood footprint. By simulating these interactions on a national scale, we identified 75 hospitals with an increase in service population greater than 30%, the typical capacity limit for German facilities. Alarmingly, one-third of these facilities are more than 10 km from the nearest flood, suggesting they may be unaware of their vulnerable position. While these represent a small fraction of the 2475 facilities in Germany, the scale and severity of disruptions they face—which have been shown to increase morbidity and mortality[10,15,36–38]—highlight the urgency of addressing such hidden risks. The ability of our method to identify such risks over large regions is one of its key advancements over previous studies. This insight provides actionable information for healthcare and transportation planners, particularly in regions where indirect effects of flooding may be overlooked.

A major strength of the framework demonstrated here is its adaptability. Although we applied the framework to Germany's healthcare-transport system, the framework can be readily adapted for other contexts and locations. The use of open-source data and a scalable gravity-based modeling framework makes this approach applicable to diverse geographic regions and infrastructure networks. This flexibility allows policymakers and healthcare administrators worldwide to use the tool for disaster scenario planning, enabling them to anticipate both direct and indirect risks posed by floods to their healthcare systems. For instance, regional decision-makers can use our interactive maps (Supplementary Data 1) to allocate resources, while facility managers can use them to assess preparedness. This aspect is particularly important in regions facing increasing frequency and severity of natural disasters due to climate change without the resources to conduct expensive local modeling.

One of the more striking findings is the identification of numerous *hidden risks*, i.e., hospitals vulnerable to indirect impacts despite being far from flood zones. Approximately one-third of the hospitals at risk of capacity exceedance in our study were located more than 10 km from the nearest flood inundation. These facilities are less likely to consider flooding as a major threat in their disaster preparedness plans, making them particularly vulnerable to the indirect effects of flooding. This result can inform strategic planning by encouraging hospitals and emergency planners to account for these indirect risks, ensuring that response resources and surge capacity are allocated appropriately.

We employ a regional-scale continuous-simulation flood model (RFM) in conjunction with a traffic model. Driven by a stochastic weather generator, RFM generates plausible flood footprints at regional scales, rather than relying on risk-based maps used by other studies. To remain computationally tractable, RFM only simulates flooding in major rivers and is too coarse to capture finer hydraulic features like embankments or bridges[61]. For example, the Rhine is parameterized as a major river only where it leaves France (around Karlsruhe, Germany), suggesting RFM under-estimates overbank flooding for 150 km of German floodplain upstream of here. Similarly, the potential for co-occurrence—particularly from seasonal events like winter river flooding in Germany[62], which aligns with peak hospital admissions due to cold-related cardiovascular conditions[63]—suggests the risks presented by this paper may be under-stated. From the 5000-year RFM simulation set, we selected 193 spatially-representative extreme events, which limits the analysis to specific events, but keeps it computationally tractable. By enhancing the resolution of these selected events, flood estimates around transportation infrastructure are more plausible; however, we do not expect the same level of accuracy as detailed local hydraulic models. To compute road or bridge failures, we rely on Germany's nationwide 5 m high-resolution mosaic of elevation data (DGM5), representing a substantial improvement in terrain resolution over previous studies[23,30,46,64,65].

To simulate traffic, we employ a macroscopic traffic model built from open-source data, capable of simulating congestion induced by rerouting at

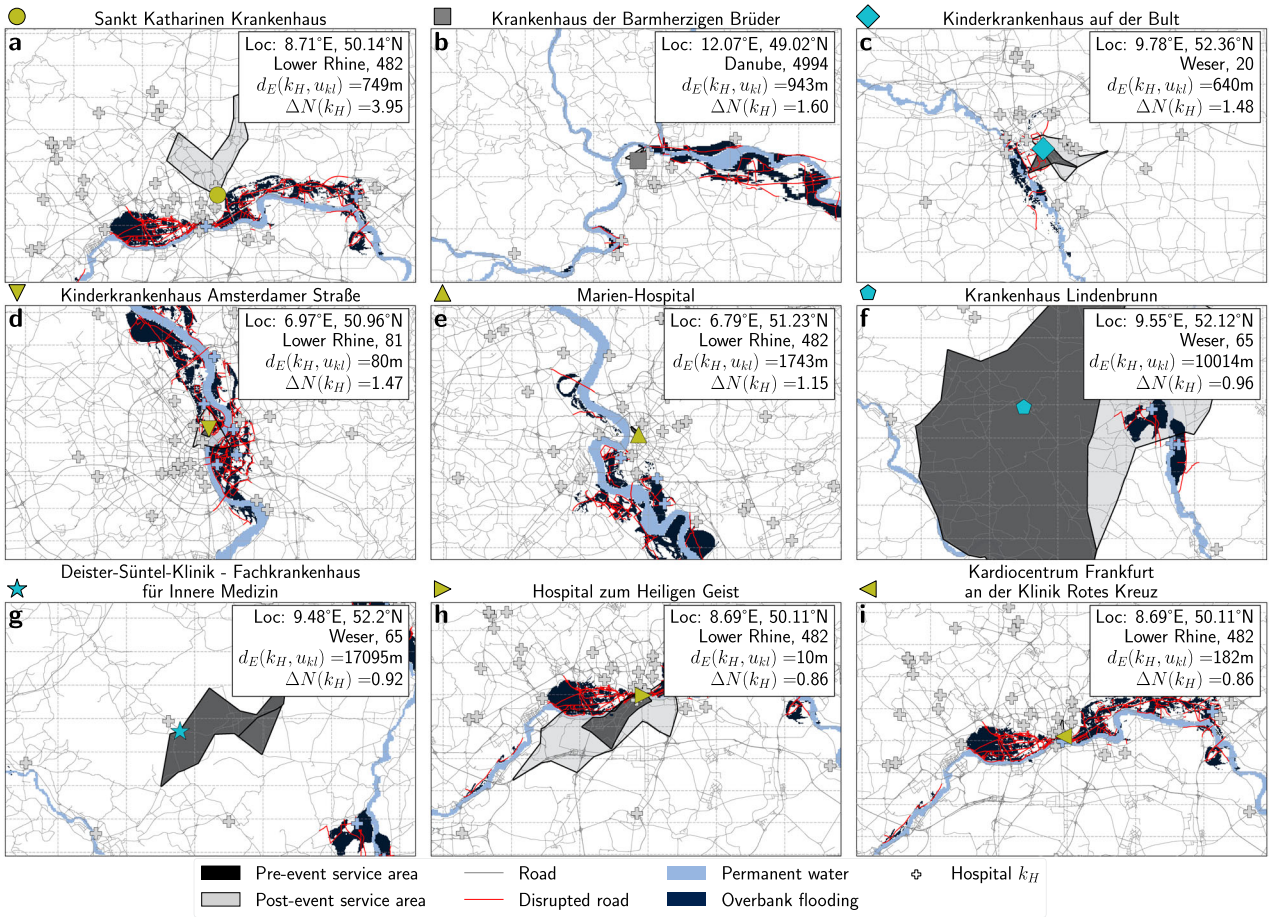

Fig. 3 | Flood-induced changes in access for nine most affected hospitals. Nine most vulnerable hospitals ranked by their change in service population, $\Delta N(k_H)$, showing the road network (gray and red lines) and the event overbank inundation (dark blue) surrounding the hospital (symbol shape corresponds to Fig 2). Other hospitals are marked with blue or gray symbols, corresponding to flooded or non-flooded facilities, respectively. Hospital service areas for the focal facility are shown for the pre- (black) and post-event conditions (gray with black outline). Note that some service areas are too small to be visible (also, the pre- and post-event areas typically overlap somewhat). Panels contain the metadata (top to bottom): location, river basin name and event number, the Euclidean distance of the facility to the nearest flooded cell $d_E(k_H, r)$ in meters, and the service population pre- and post-flood event, N_{pre} & N_{pre}, respectively. See text for discussion of panel **a**–**i** and Supplementary Data 1 for interactive maps of these scenarios.

a national scale. To accomplish this, we assume optimal decision-making by drivers, excluding factors like Emergency Medical Service vehicles' ability to bypass congestion or non-vehicular transport methods such as helicopters. Cross-border healthcare decisions are similarly excluded, despite their importance in transnational contexts. Moreover, the use of a 30 cm threshold for road disruption omits other factors that influence such performance under hydraulic loading like debris and flow velocity. Related to this, we are unable to estimate the duration of such disturbances; however, experience from recent 2021 flooding in Germany suggests temporary bridges can be installed in two to seven days[66,67] while full reconstruction can last more than three years[68].

Our analysis focused on hospitals, a subset of all healthcare facilities, as hospitals are uniquely embedded within Germany's legal, infrastructure, and disaster response systems. For example, only hospitals are included in state healthcare planning and receive infrastructure funding under the Hospital Financing Act ("KHG")[69]. In contrast to outpatient facilities, their bed capacity and surge potential are formally tracked and regulated[70], making hospitals critical for healthcare resilience, particularly under transportation disruptions. Furthermore, hospitals provide high-acuity services—such as emergency, surgical, and intensive care—that are more relevant to disaster response than the services typically offered by smaller or outpatient facilities. While hospitals are central to disaster response, other facilities in Germany such as medical care centers ("Medizinische Versorgungszentren"), general practitioner practices ("Hausarztpraxen"), and specialist practices ("Facharztpraxen") can provide valuable support during the recovery phase by treating stable patients, delivering routine medical care, and thereby relieving pressure on hospital-based emergency services[71]. If such facilities were included in the analysis, we expect the urban-rural disparities reported elsewhere (e.g., reduced accessibility to neurological care in rural areas[72]) would be even more pronounced. This is because outpatient facilities are more densely concentrated in urban areas and could help compensate for the loss of hospital services. However, this buffering effect would be more relevant for long-term care needs rather than for acute care disruptions.

Our traffic-simulation framework prioritizes computational efficiency and aggregate behavior, a necessary trade-off between model complexity and tractability at the national scale and within our available computational resources. Incorporating stochastic elements—such as probabilistic route choice to capture uncertainty in driver behavior, or stochastic hospital selection to reflect variability in preferences and capacity constraints—could enhance model realism and policy relevance. Future studies focused on smaller geographic regions or supported by greater computational resources could explore these more sophisticated approaches; however, such benefits must be carefully weighed against the increased complexity and computational burden.

For our analysis, we assumed high traffic congestion (γ = 0.1) after Wassmer et al.[33] to focus on the peak traffic periods when flood-induced

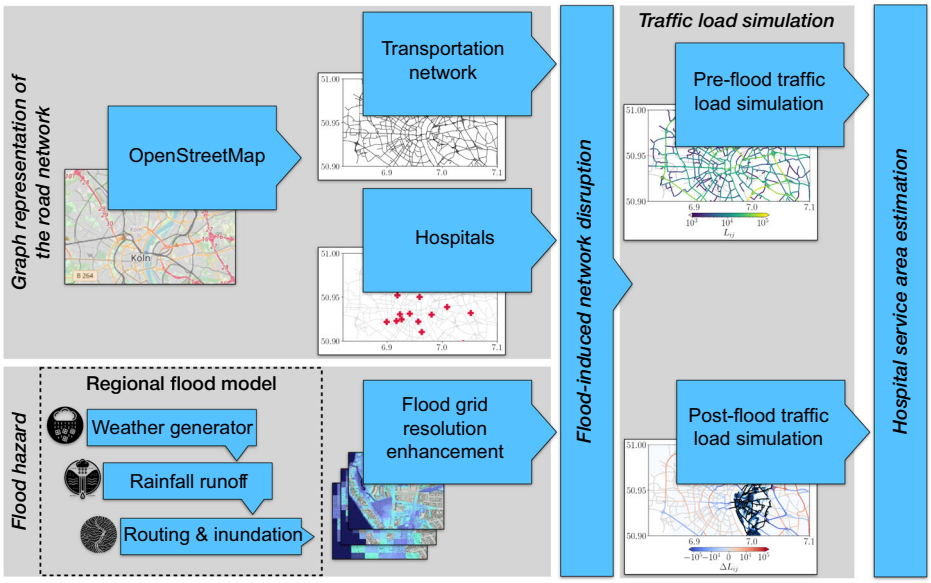

Fig. 4 | Study workflow summary. Study workflow summary and framework for estimating the vulnerability of hospitals to flood-induced transportation disruptions. Blue arrows denote the flow of information between steps and *emphasized text* relates to specific sub-sections where details are provided.

disruptions are most critical. To test the sensitivity of this assumption, Supplementary Discussion 1 presents a comparison of the modeled affected facility counts and distance to nearest inundation estimates for a range of γ values. This comparison shows that as congestion increases, more facilities are affected by the flood disruption, and their average distance to flooding increases. While the overall sensitivity of γ is moderate (roughly 50% change in affected facility count for the range considered), these findings demonstrate the importance of considering traffic and congestion in the analysis of flood-driven hospital impacts.

To develop a comprehensive dataset of hospital locations, we opted to use OpenStreetMap (OSM) data for its global coverage, structured classification, and compatibility with our cross-border analysis. While OSM struggled with completeness historically (and continues to be problematically sparse in some regions outside of Europe), Herfort et al.[73] found building footprints to be over 80% complete for most locations tested in Germany. Alternatively, the official hospital directory ("Krankenhausverzeichnis") could be used[74]; however, it only covers Germany, lacks coordinate data (providing only addresses, some of which are missing or incorrect), and does not differentiate between hospitals and clinics, limiting its utility for spatially-explicit and cross-border healthcare accessibility modeling.

Using the pre- and post-flood traffic load simulations, we provide an analysis of indirect flood impacts on 2475 hospitals servicing Germany. To estimate these impacts, we use increases in relative service population ($\Delta N(k_H)$) as an indicator, while acknowledging that this metric omits certain factors that relate it to actual patient loads. For instance, we do not account for sub-optimal facility distribution, such as hospitals with baseline capacities that have not been adjusted to reflect recent nearby population increases. Additionally, sub-optimal decision-making by patients—who may not know which hospital is nearest or most appropriate for their needs—is not considered. We also omit hidden facility preferences, where patients might prefer certain service providers and are willing to endure longer travel times to access them. Furthermore, we assume homogeneous acuity among hospitals, implying that disruptions at one facility can be absorbed by nearby hospitals, which overlooks the variability in hospital specialization and capacity. In reality, higher-acuity hospitals, which provide specialized care, are less replaceable, and disruptions at these facilities could lead to more severe consequences[75]. Similarly, the model does not account for cascading failures, such as when overwhelmed facilities turn away patients, which could further compound the problem. Regardless, $\Delta N(k_H)$ provides a transparent quantitative indicator of traffic-related hospital load changes that decision-makers can use to inform resilience plans and identify system vulnerabilities at a national scale. Future research should consider implementing our approach on a European scale to yield broader insights, incorporating future climate scenarios and simulating future infrastructure growth to provide more comprehensive risk assessments, adopting a multi-hazard approach that encompasses other disasters beyond floods to offer a more holistic perspective, and incorporating variations in hospital acuity levels to better capture the nuanced impacts of disruptions.

Although our approach focuses on assessing impacts rather than prescribing interventions, it offers a valuable decision-support tool for resilience planning. To support the translation of our findings into actionable insights, we provide interactive maps in Supplementary Data 1 for the 75 most affected facilities. These maps are intended to help local stakeholders visualize where the most severe disruptions occur, guiding targeted efforts to reduce vulnerability and improve access during future flood events. Future work could expand our framework by integrating optimization routines to evaluate infrastructure and healthcare interventions—such as adding road links, increasing facility capacity, or dispatching emergency services—under specific budget constraints, with the goal of maximizing accessibility and minimizing service disruption.

Conclusions

In conclusion, this study highlights the critical vulnerabilities of healthcare systems to the indirect impacts of flooding, emphasizing the crucial role of transportation networks and trans-boundary dynamics in disaster resilience. Our integrated framework, designed for reproducibility and scalability, combines a high-resolution flood model with a gravity-based traffic model. Applied to Germany, it demonstrates how flood-related disruptions can lead to increased strain on hospitals far from flood zones through increased patient loads. The identification of *hidden risks*—facilities vulnerable to indirect disruptions despite being distant from floodwaters—underscores the need for comprehensive, system-wide resilience planning. The adaptability of this framework makes it a valuable tool for planners globally, especially as climate change increases the frequency and severity of natural disasters. By incorporating these insights into disaster planning, healthcare systems can better prepare for the complex challenges posed by floods, ensuring resilience and reducing the risk of overwhelming patient surges during crises.

Methods

To quantify healthcare-transport system vulnerability to flooding, we develop the simulation-based method summarized in Fig. 4 and elaborated in the following sections.

Flood hazard

To provide the flood hazard information used as forcings in our post-flood traffic modeling, we used simulated maximum event flood water surface depths or heights (WSH) from the process-based continuous-simulation *Regional Flood Model* (RFM) of Sairam et al.[61]. RFM linked three submodels to simulate flooding within the major river basins of Germany: a weather generator to simulate realistic rainfall fields, a hydrological model to translate rainfall into streamflow, and a coupled 1D-2D hydrodynamic model to simulate in-channel kinematics and overbank flooding[76]. The 2D hydrodynamic overbank flooding submodel employed a 100 m digital elevation model (DEM) constructed by aggregating via averaging the 10 m DEM from BKG[77]. To facilitate parallel computations, RFM was spatially discretized by Germany's five major river basins (see Supplementary Fig. 1) within which flood events were defined by periods where simulated water levels exceeded levee crest heights (using a rolling 10-day threshold to separate events). With this framework,[61] simulated 5000 years of weather from the current climate yielding roughly 20,000 flood events spread across the five basins (see Supplementary Table 2). Simulating this complete set of events using our traffic model (see below) would require approximately $\mathcal{O}(10^6)$ core-hours.

To reduce this computational burden through additional parallelization of the traffic model, we divided the large Danube and Rhine RFM basins in-two using political boundaries, yielding a total of seven analysis basins as shown in Supplementary Fig. 1. For further simplification, we employed an *event selection routine* to identify a spatially-representative sub-set of the original 20,000 RFM events by selecting those with the highest wet-cell count for each local region within Germany (see Supplementary Methods 1). When applied to the original 20,000 RFM event set, this routine yielded 193 *analysis events* divided among the seven analysis basins as summarized in Supplementary Table 2 and provided in ref. 78.

To improve the sampling of the WSH grid, we transformed the RFM native 100 m maximum WSH grid from each analysis event to a finer 5 m grid using a modified version of the *CostGrow* algorithm from Bryant et al.[79] and the "Digitales Geländemodell Gitterweite 5 m" (DGM5) DEM dataset[80]. This approach uses computationally efficient hydraulic assumptions to better represent the inundation of sub-100 m topographic features, like roads, and is further described in Supplementary Methods 2 along with a sensitivity analysis demonstrating the advantage of the enhancement. The resulting 5 m grids are provided in Bryant[81] and are similar in resolution to previous local-scale studies (e.g., 1 m[82] and 5 m[29,83]), indicating an improvement our regional study makes over studies of a similar macro-scale (e.g., 30 m[64], 50 m[46], 100 m[23,30] and 1000 m[65]). While this enhancement increased the memory footprint by a factor of 70, an evaluation of an event within the Ems basin (Supplementary Methods 2) suggests that this enhancement substantially improves the road disruption calculation.

Graph representation of the road network

Following the methodology of Wassmer et al.[33], we constructed road networks using OpenStreetMap (OSM) data to construct a directed graph $G(V, E)$ where edges E represent road segments and nodes V denote road intersections or endpoints. These road segments E include major roads (defined with an OSM query on the *highway* key with any value including *motorway*, *trunk*, *primary*, *secondary*, *tertiary* or *unclassified*) as other road types substantially increase graph size while having a negligible influence on the overall traffic flow[33]. To assign a population count N_i to each node $i \in V$ we allocate population data from the Global Human Settlement Layer[84] (100 m resolution), weighting every node by the area of its respective Voronoi polygon. This weight provides population values and enables every node in the road network to serve as a potential origin or destination for a journey. To evaluate the healthcare system in particular, the nodes nearest to a hospital location (OSM key *amenity* = *hospital*) were further denoted as $k_H \in V$. From this network, the shortest path P is identified by selecting the combination of edges (ij) which minimizes the total travel time t_{nm} between two nodes n and m defined as:

$$t_{nm} = \min\left\{\sum_{(i,j)\in P} t_{ij}\right\}, \tag{1}$$

where t_{ij} is the travel time on edge (ij), which we calculated using the maximal velocities and the road lengths provided by OSM.

Following this approach, we created a road graph for each analysis basin plus a 75 km buffer to reduce boundary effects after Wassmer et al.[33] (see Supplementary Fig. 1 for the analysis basins and Supplementary Data 1 for an example road graph). The resulting graph sizes range from ~110,000 nodes and ~250,000 edges for the upper Elbe basin to ~420,000 nodes and ~920,000 edges for the lower Rhine basin. The complete graphs are provided in ref. 85.

Flood-induced network disruption

To assess the impact of a flood event on the road network, we compared simulations from the pre-flood road network $G(V, E)$ against those from the post-flood road network $G_r(V, E\backslash E_f)$, where E_f is the road segments or edges made impassable by the flood. To determine E_f, we sampled the WSH grids using each road segment for each analysis event to determine the road segment flood depth. Segments with flood depths exceeding 0.3 m were considered disrupted after Pregnolato et al.[29] and therefore included in E_f. For this calculation, we assumed an equivalent datum for road crest height and WSH values, with the exception of elevated and subterranean structures (i.e., bridges and tunnels respectively). Such special structures were included in E_f only if the WSH values sampled at the access or entry points were greater than 0.3 m (see Supplementary Methods 3 for details and Supplementary Fig. 3 for an example). Based on this treatment of road segments or edges, it follows that nodes V can be considered disrupted or flooded if all incident edges are flooded. In our analysis, we assume the population attributed to such nodes has been forced to relocate, and should therefore be excluded from the scenario. In particular, a facility is shown as "flooded" (e.g., on Fig. 3) if all access roads are inundated, reducing its service population to zero and effectively removing it from the scenario.

Traffic load simulation

To simulate traffic within the parameterized transportation network, we employed a gravity-based traffic model after Wassmer et al.[33]. This model assumes that the flow of travelers is defined as the origin population (N_n) times the normalized (population-weighted) probability of travelers going to a destination m or:

$$F_{nm} = N_n \cdot \frac{N_m P(t_{nm})}{\sum_{k\in V} N_k P(t_{nk})}, \tag{2}$$

where $P(t_{nk})$ is the probability of a traveler going from the origin n to some destination k given the travel time, N_k is the population for each node k which is an element of V.

To estimate the load or number of vehicles on a single edge or road segment (ij) under free-flow conditions considering *all* possible origin n and destination m pairs, this flow of travelers is multiplied by the ratio of the count of shortest-paths traversing (ij) ($\sigma(n, m)$) over the total number of shortest-paths between n and m in the network ($\sigma(n, m|(ij))$):

$$L_{ij} = \sum_{n,m} \frac{\sigma(n, m|(ij))}{\sigma(n, m)} F_{nm}. \tag{3}$$

In effect, this equation assumes every driver follows the shortest path based on free-flow conditions and has no knowledge of the current system state (i.e., drivers do not have real-time traffic information, such as from Google Maps). This approach captures key first-order congestion effects while remaining computationally tractable for our large-scale analysis.

To account for congestion or vehicle interaction delays, a reduction factor was applied to Equation (3) (see ref. 33) yielding the effective travel

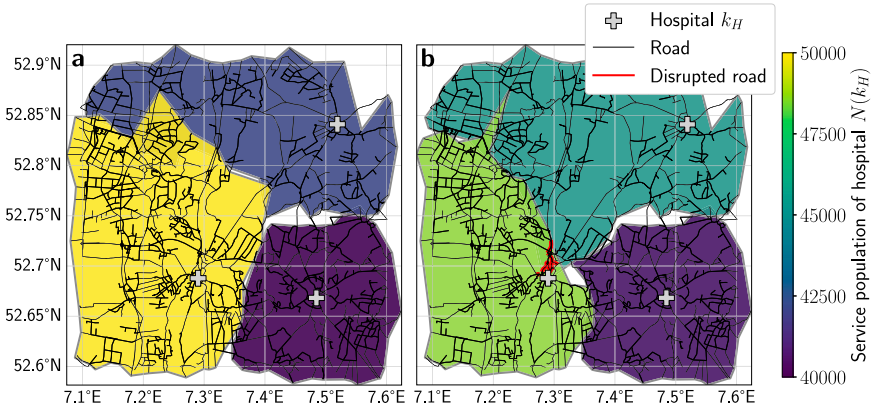

Fig. 5 | Hospital service area disruption example. Hospital service area in an example region: **a** pre-flooding event and **b** post-flooding event, where some roads were flooded and removed from the road network (red). The service area of a hospital (light-gray plus symbol) is defined as the region within which the shortest path distance from any node to that particular facility is less than the distance to any other facility (gray border). The service population for a hospital is defined by the population within its 5 nearest hospitals (color coding; see Eq. (5)).

time:

$$t_{ij}^{\text{eff}}(L_{ij}) = L_{ij} \cdot \frac{\gamma t_r l_{ij}}{l_{ij} m_{ij} - \gamma d_c L_{ij}} \in [t_{ij}^{\min}, t_{ij}^{\max}], \tag{4}$$

where l_{ij} and m_{ij} are the lengths and number of lanes respectively of edge (ij) taken from OSM, $d_c = 5\ m$ is the typical length of a vehicle, $t_r = 2\ s$[86] is the the reaction time or the average time taken for a vehicle to arrive at the current position of its predecessor, and γ characterizes the traffic magnitude in the system. It is further constrained between a minimum value $t_{ij}^{\min}$, determined by the free-flow travel time based on road segment length and speed limit, and a maximum value $t_{ij}^{\max}$ corresponding to the time required to traverse the segment at walking speed ($v_{\min} = 5\ \text{km h}^{-1}$). This equation expresses the effective travel time t_{ij}^{eff} of an edge (ij) as a function of the traffic load L_{ij} adjusted for congestion effects through an occupancy-based delay factor. This factor depends on driver behavior (via reaction time and car length), the attributes of the edge (length, number of lanes, and speed limit), and the traffic magnitude parameter γ. This traffic magnitude parameter γ represents the overall network load or congestion level, where a γ of zero equates to a road network with no vehicle interactions (i.e., free-flow travel). While parameterizing γ is challenging due to its spatiotemporal variability and limited empirical data, analysis from the German Mobility Panel suggests that $\gamma = 0.1$ corresponds to high-congestion conditions typically observed during rush hours[33,87]. We adopted this value to reflect peak traffic periods when flood-induced disruptions are likely to have the most severe impacts on hospital accessibility (see Supplementary Discussion 1 for a sensitivity analysis of this parameter).

Hospital service area estimation

We analyzed the impact of flood-related traffic disruptions by delineating facility service populations and areas, defined as the potential patients of a facility and likely geographic regions served by each facility respectively. To estimate the service population for each facility k_H, we took the "expected value" of service population computed as:

$$N(k_H) = \sum_{n \in V} p_n^{k_H} N_n, \tag{5}$$

where N_n is population at node n, and $p_n^{k_H}$ is the probability of node n visiting facility k_H. To reflect our assumption that potential patients are more likely to visit hospitals that are nearby, $p_n^{k_H}$ was estimated using the normalized inverse distance:

$$p_n^{k_H} = \frac{1}{t_{nk_H}^{\text{eff}}} \left(\sum_{k \in K} \frac{1}{t_{nk}^{\text{eff}}} \right)^{-1}, \tag{6}$$

where $K \subset V$ is the set of κ hospitals nearest to a node n. The use of $\kappa > 1$ reflects the uncertainty in predicting which hospital a patient may be transported to. This uncertainty is especially high in urban areas where many hospitals may have similar travel times. For the present study, we found $\kappa > 5$ to increase boundary effects and computational burden; therefore, $\kappa = 5$ was adopted. This approach does not consider other factors that may influence patient decisions like facility acuity or specialization, hidden preferences, or sub-optimal decision making.

While hospital service population $N(k_H)$ provides a useful quantitative metric for evaluating system vulnerability, it can be difficult to visualize, especially in the mapping exercises common in disaster planning. To support such visualization, we further estimated each facility's service area by grouping all nodes where k_H was found to be the nearest according to Eq. (1) into a set of mutually exclusive polygons. These service areas simply indicate those nodes which are nearest to a given hospital, irrespective of the neighboring facilities included in the $\kappa = 5$ of Eq. (6). Therefore, the service population $N(k_H)$ may change even in scenarios where the service area does not.

To illustrate our calculation of service population changes, consider an example with three neighboring hospitals. Initially, each facility serves a distinct area and population based on the existing pre-flood road network connectivity and travel time as shown in Fig. 5 panel a. Now, envision a post-flood situation where a flood disrupts portions of the road network (red lines; panel b), altering accessibility to these facilities. This disruption reduces the accessibility of one facility—specifically, the one located in the lower-left region—thereby decreasing its service area and population. Consequently, patients are redistributed to neighboring facilities, such as the one in the upper-right region, which experience an increase in service area and population. These changes are represented by differences in polygon shapes and colors (indicating service areas and populations respectively) between the two panels in Fig. 5. We quantify this relative service population change as:

$$\Delta N(k_H) = \frac{N_{\text{post}}(k_H) - N_{\text{pre}}(k_H)}{N_{\text{pre}}(k_H)}, \tag{7}$$

where $N_{\text{pre}}(k_H)$ and $N_{\text{post}}(k_H)$ are the service populations of hospital k_H before and after a disruptive flood event, respectively.

Calculated in this way, important attributes of a local healthcare-transport system's vulnerability to indirect flood impacts can be studied. For example, $\Delta N(k_H) > 0$ indicates a hospital's service population has increased because roads leading to neighboring hospitals are disrupted or congested, or if neighboring facilities are disabled. Specifically, a value of $\Delta N(k_H) > 1$ indicates that service populations have more than doubled. Understanding how $\Delta N(k_H)$ changes in response to flood disturbances can help identify weak points and opportunities for mitigation.

Data availability

Data used in this study related to the traffic model, including road network data, hospital locations, and model input files, are provided in ref. 85. The

flood events selected from RFM are provided in ref. 78 and the downscaled results in ref. 81. Road network data as well as hospital location data are based on OpenStreetMap extracts retrieved via the Geofabrik service[88] and processed as described in the Methods. Population data were obtained from the Global Human Settlement Layer[84], and mobility data were retrieved from the German Mobility Panel[89].

Code availability

The code used to conduct the traffic analysis and generate the results in this study is provided[85]. The downscaling tool is provided in ref. 90.

Received: 19 November 2024; Accepted: 30 July 2025;
Published online: 18 August 2025

References

1. Van Minh, H. et al. Primary healthcare system capacities for responding to storm and flood-related health problems: a case study from a rural district in central Vietnam. *Glob. Health Action* **7**, 23007 (2014).
2. Rattanakanlaya, K., Sukonthasarn, A., Wangsrikhun, S. & Chanprasit, C. A survey of flood disaster preparedness among hospitals in the central region of Thailand. *Australas. Emerg. Nurs. J.* **19**, 191–197 (2016).
3. Valente, M. et al. Health system response to the 2023 floods in Emilia-Romagna, Italy: a field report. *Prehosp. Disaster Med.* **38**, 813–817 (2023).
4. Curiel, T. J. Murder or mercy? hurricane katrina and the need for disaster training. *N. Engl. J. Med.* **355**, 2067–2069 (2006).
5. Fonseca, V. A. et al. Impact of a natural disaster on diabetes: exacerbation of disparities and long-term consequences. *Diab. Care* **32**, 1632–1638 (2009).
6. Bell, S. A., Klasa, K., Iwashyna, T. J., Norton, E. C. & Davis, M. A. Long-term healthcare provider availability following large-scale hurricanes: a difference-in-differences study. *PLOS One*. **15**, e0242823 (2020).
7. Rathnayake, D., Clarke, M. & Jayasinghe, V. I. Health system performance and health system preparedness for the post-pandemic impact of COVID-19: a review. *Int. J. Healthc. Manag.* **14**, 250–254 (2021).
8. Alderman, K., Turner, L. R. & Tong, S. Floods and human health: a systematic review. *Environ. Int.* **47**, 37–47 (2012).
9. Hick, J. L., Hanfling, D., Wynia, M. K. & Pavia, A. T. Duty to plan: Health care, crisis standards of care, and novel coronavirus SARS-CoV-2. *NAM Perspect*. https://doi.org/10.31478/202003b (2020).
10. Sartini, M. et al. Overcrowding in emergency department: causes, consequences, and solutions—a narrative review. *Healthcare* **10**, 1625 (2022).
11. Phillips, J. L. et al. Overcrowding and its association with patient outcomes in a median-low volume emergency department. *J. Clin. Med. Res.* **9**, 911 (2017).
12. Hsuan, C., Segel, J. E., Hsia, R. Y., Wang, Y. & Rogowski, J. Association of emergency department crowding with inpatient outcomes. *Health Serv. Res.* **58**, 828–843 (2023).
13. Dorvil, S. et al. Disruption of healthcare in New York City during the COVID-19 pandemic: Findings from residents living in north and central Brooklyn, the south Bronx, and East and central Harlem. *J. Prim. Care Community Health* **14**, 21501319231205992 (2023).
14. Clements, A. et al. Overcrowding and understaffing in modern health-care systems: key determinants in meticillin-resistant Staphylococcus aureus transmission. *Lancet Infect. Dis.* **8**, 427–434 (2008).
15. Jena, A. B., Mann, N. C., Wedlund, L. N. & Olenski, A. Delays in emergency care and mortality during major us marathons. *N. Engl. J. Med.* **376**, 1441–1450 (2017).
16. Huelskoetter, T. Hurricane Katrina's health-care legacy, https://www.americanprogress.org/article/hurricane-katrinas-health-care-legacy/ (2015).
17. Wei, S. Y. How does the effect of Hurricane Katrina influence health-care infrastructure and resilience? https://pdxscholar.library.pdx.edu/honorstheses/927 (2020).
18. Shoaf, K. Organizing the health sector for response to disasters. *Ciência Saúde. Coletiva* **19**, 3705–3715 (2014).
19. Djalali, A. et al. Art of disaster preparedness in European Union: a survey on the health systems. *PLoS Curr.* **6**, ecurrents.dis.56cf1c5c1b0deae1595a48e294685d2f (2014).
20. Meyer, D. et al. A checklist to improve health system resilience to infectious disease outbreaks and natural hazards. *BMJ Glob. Health* **5**, e002429 (2020).
21. Ebi, K. L. et al. Extreme weather and climate change: population health and health system implications. *Annu. Rev. Public Health* **42**, 293–315 (2021).
22. Alabbad, Y., Mount, J., Campbell, A. M. & Demir, I. Assessment of transportation system disruption and accessibility to critical amenities during flooding: Iowa case study. *Sci. Total Environ.* **793**, 148476 (2021).
23. Koks, E. E. et al. A global multi-hazard risk analysis of road and railway infrastructure assets. *Nat. Commun.* **10**, 2677 (2019).
24. Schuster, H., Polleres, A. & Wachs, J. Stress-testing road networks and access to medical care. *Transp. Res. Part A Policy Pract.* **181**, 104017 (2024).
25. Gangwal, U. & Dong, S. Critical facility accessibility rapid failure early-warning detection and redundancy mapping in urban flooding. *Reliab. Eng. Syst. Saf.* **224**, 108555 (2022).
26. Abebe, Y. A., Pregnolato, M. & Jonkman, S. N. Flood impacts on healthcare facilities and disaster preparedness – a systematic review. *Int. J. Disaster Risk Reduct.* **119**, 105340 (2025).
27. Weeks, E. A. Lessons from Katrina: Response, recovery and the public health infrastructure. *DePaul J. Health Care Law* **10**, 251–290 (2007).
28. Voss, M., Rüger, A., Bock, N., Dittmer, C. & Merkes, S. T. Die evakuierung des st.-antonius-hospitals eschweiler während der flutereignisse im juli 2021. KFS Working Paper 25, Katastrophenforschungsstelle (KFS), Freie Universität Berlin, https://refubium.fu-berlin.de/handle/fub188/35555 (2022).
29. Pregnolato, M., Ford, A., Wilkinson, S. M. & Dawson, R. J. The impact of flooding on road transport: a depth-disruption function. *Transp. Res. Part D Transp. Environ.* **55**, 67–81 (2017).
30. van Ginkel, K. C. H., Dottori, F., Alfieri, L., Feyen, L. & Koks, E. E. Flood risk assessment of the European road network. *Nat. Hazards Earth Syst. Sci.* **21**, 1011–1027 (2021).
31. Pregnolato, M., Ford, A., Glenis, V., Wilkinson, S. & Dawson, R. Impact of climate change on disruption to urban transport networks from pluvial flooding. *J. Infrastruct. Syst.* **23**, 04017015 (2017).
32. Mitchell, M., Hendricks, J. & Schatt, D. Road network analyses elucidate hidden road flooding impacts under accelerating sea level rise. *Front. Environ. Sci.* **11**, https://www.frontiersin.org/articles/10.3389/fenvs.2023.1083282 (2023).
33. Wassmer, J., Merz, B. & Marwan, N. Resilience of transportation infrastructure networks to road failures. *Chaos* **34**, 013124 (2024).
34. Affleck, A. & Gibbon, J. Workington: a case study in coordination and communication. *Proc. Inst. Civ. Eng. Municipal Eng.* **169**, 109–117 (2016).
35. Zhang, Y. et al. Spatial accessibility of emergency medical services under inclement weather: a case study in Beijing, China. *Nat. Hazards Earth Syst. Sci.* **24**, 63–77 (2024).
36. Kuntz, L., Mennicken, R. & Scholtes, S. Stress on the ward: evidence of safety tipping points in hospitals. *Manag. Sci.* **61**, 754–771 (2015).
37. Boyle, A., Higginson, I., Sarsfield, K. & Kumari, P. Rcem acute insight series: crowding and its consequences. https://rcem.ac.uk/wp-

content/uploads/2021/11/RCEM_Why_Emergency_Department_Crowding_Matters.pdf (2021).
38. Song, J., Chen, C., Zhao, S., Zhou, L. & Chen, H. Trading quality for quantity? Evidence from patient level data in China. *PLOS ONE*. **16**, e0257127 (2021).
39. Nagel, K. & Schreckenberg, M. A cellular automaton model for freeway traffic. *J. de. Phys. I* **2**, 2221–2229 (1992).
40. Nguyen, J., Powers, S. T., Urquhart, N., Farrenkopf, T. & Guckert, M. An overview of agent-based traffic simulators. *Transp. Res. Interdiscip. Perspect.* **12**, 100486 (2021).
41. Ziemke, D., Kaddoura, I. & Nagel, K. The Matsim Open Berlin Scenario: aa multimodal agent-based transport simulation scenario based on synthetic demand modeling and open data. *Proc. Comput. Sci.* **151**, 870–877 (2019).
42. W Axhausen, K., Horni, A. & Nagel, K. *The multi-agent transport simulation MATSim* (Ubiquity Press, 2016).
43. Lopez, P. A. et al. Microscopic traffic simulation using SUMO. In *The 21st IEEE International Conference on Intelligent Transportation Systems* (IEEE, 2018). https://elib.dlr.de/124092/.
44. Burghout, W., Koutsopoulos, H. N. & Andreasson, I. Hybrid mesoscopic–microscopic traffic simulation. *Transp. Res. Rec.* **1934**, 218–225 (2005).
45. Aw, A., Klar, A., Rascle, M. & Materne, T. Derivation of continuum traffic flow models from microscopic follow-the-leader models. *SIAM J. Appl. Math.* **63**, 259–278 (2002).
46. Yu, D. et al. Disruption of emergency response to vulnerable populations during floods. *Nat. Sustain.* **3**, 728–736 (2020).
47. Dong, S., Gao, X., Mostafavi, A. & Gao, J. Modest flooding can trigger catastrophic road network collapse due to compound failure. *Commun. Earth Environ.* **3**, 1–10 (2022).
48. Coles, D., Yu, D., Wilby, R. L., Green, D. & Herring, Z. Beyond 'flood hotspots': Modelling emergency service accessibility during flooding in York, UK. *J. Hydrol.* **546**, 419–436 (2017).
49. Dafermos, S. C. & Sparrow, F. T. The traffic assignment problem for a general network. *J. Res. Natl Bur. Standards: Math. Sci. B* **73**, 91 (1969).
50. Erlander, S. & Stewart, N. F. *The gravity model in transportation analysis: theory and extensions*, 3 (Vsp, 1990).
51. Dahlmanns, M., Kaiser, F. & Witthaut, D. Branching in flow networks with linear congestion. *Phys. Rev. Res.* **4**, 043208 (2022).
52. Reilly, W. J. *The Law of Retail Gravitation*, 2 edn. (W. J. Reilly, Inc., 1953).
53. Letouzé, E., Purser, M., Rodríguez, F. & Cummins, M. Revisiting the migration-development nexus: a gravity model approach. MPRA Paper, University Library of Munich, Germany (2009).
54. Krings, G., Calabrese, F., Ratti, C. & Blondel, V. D. Urban gravity: a model for inter-city telecommunication flows. *J. Stat. Mech. Theory Exp.* **2009**, L07003 (2009).
55. Petricola, S., Reinmuth, M., Lautenbach, S., Hatfield, C. & Zipf, A. Assessing road criticality and loss of healthcare accessibility during floods: the case of cyclone Idai, Mozambique 2019. *Int. J. Health Geographics* **21**, 14 (2022).
56. Metin, A. D. et al. The role of spatial dependence for large-scale flood risk estimation. *Nat. Hazards Earth Syst. Sci.* **20**, 967–979 (2020).
57. Green, D. et al. City-scale accessibility of emergency responders operating during flood events. *Nat. Hazards Earth Syst. Sci.* **17**, 1–16 (2017).
58. Ganin, A. A. et al. Resilience and efficiency in transportation networks. *Sci. Adv.* **3**, e1701079 (2017).
59. Schehadat, M. S., Groneberg, D. A., Bauer, J. & Bendels, M. H. K. Hilfsfristen des Rettungsdienstes in den deutschen Bundesländern. *Zentralblatt Arbeitsmedizin Arbeitsschutz und Ergonomie* **67**, 255–260 (2017).
60. Bölt, U. Statistische krankenhausdaten: Grunddaten der krankenhäuser 2020. In *Krankenhaus-Report 2023: Schwerpunkt: Personal*, 353–380 (Springer, 2023).
61. Sairam, N. et al. Process-based flood risk assessment for Germany. *Earths Fut.* **9**, e2021EF002259 (2021).
62. Hall, J. & Blöschl, G. Spatial patterns and characteristics of flood seasonality in Europe. *Hydrol. Earth Syst. Sci.* **22**, 3883–3901 (2018).
63. Shiue, I., Perkins, D. R. & Bearman, N. Hospital admissions due to diseases of arteries and veins peaked at physiological equivalent temperature -10 to 10 °C in Germany in 2009–2011. *Environ. Sci. Pollut. Res.* **23**, 6159–6167 (2016).
64. Panakkal, P., Wyderka, A. M., Padgett, J. E. & Bedient, P. B. Safer this way: identifying flooded roads for facilitating mobility during floods. *J. Hydrol.* **625**, 130100 (2023).
65. Zhou, Y., Liu, K. & Wang, M. River flood risk assessment for the Chinese road network. *Transp. Res. Part D Transp. Environ.* **121**, 103818 (2023).
66. Deutsche Presse-Agentur. Erste Behelfsbrücke über die Ahr in Betrieb (2021).
67. University of the German Armed Forces. Professoren der UniBw M zur Begutachtung von Behelfsbrücken im Ahrtal. https://www.unibw.de/home/news/2021/hochwassereinsatz-professoren-der-unibw-m-zur-begutachtung-von-behelfsbruecken-im-ahrtal (2021).
68. Landesbetrieb Straßenbau Nordrhein-Westfalen. L136: Neubau der Rurbrücke Jülich bis Sommer 2024. https://www.strassen.nrw.de/de/meldung/l136-neubau-der-rurbruecke-juelich-bis-fruehjahr-2024.html (2023).
69. Regierungskommission für eine moderne und bedarfsgerechte Krankenhausversorgung. Dritte Stellungnahme und Empfehlung der Regierungskommission für eine moderne und bedarfsgerechte Krankenhausversorgung: Grundlegende Reform der Krankenhausvergütung [Third Opinion and Recommendation of the Government Commission for Modern and Demand-Oriented Hospital Care: Fundamental Reform of Hospital Remuneration]. Bundesministerium für Gesundheit, Berlin https://www.bundesgesundheitsministerium.de/krankenhauskommission-stellungnahme-krankenhausverguetung.pdf (2022).
70. Reif, S. & Schubert, S. Hospital capacity reporting in Germany during Covid-19. *J. Econ. Behav. Organ.* **228**, 106730 (2024).
71. Hecker, N. & Domres, B. D. The German emergency and disaster medicine and management system—history and present. *Chin. J. Traumatol.* **21**, 64–72 (2018).
72. Bauer, J., Klingelhöfer, D., Maier, W., Schwettmann, L. & Groneberg, D. A. Spatial accessibility of general inpatient care in Germany: an analysis of surgery, internal medicine and neurology. *Sci. Rep.* **10**, 19157 (2020).
73. Herfort, B., Lautenbach, S., Porto de Albuquerque, J., Anderson, J. & Zipf, A. A spatio-temporal analysis investigating completeness and inequalities of global urban building data in OpenStreetMap. *Nat. Commun.* **14**, 3985 (2023).
74. Statistisches Bundesamt (Destatis). Krankenhausverzeichnis nach §293 absatz 6 sgb v - krankenhäuser in der bundesrepublik deutschland. Version: 01.02.2025. Herausgeber: Statistisches Bundesamt (Destatis), Fachbereich 12 Gesundheitswesen, https://www.destatis.de, https://www.destatis.de/DE/Themen/Gesellschaft-Umwelt/Gesundheit/Krankenhaeuser/krankenhausverzeichnis.html (2025).
75. Law, A. C. et al. Patient outcomes after long-term acute care hospital closures. *JAMA Netw. Open* **6**, e2344377 (2023).
76. Falter, D. et al. Continuous, large-scale simulation model for flood risk assessments: Proof-of-concept: Large-scale flood risk assessment model. *J. Flood Risk Manag.* **9**, 3–21 (2016).
77. BKG. Digitales Geländemodell Gitterweite 10 m. [Dataset, https://gdz.bkg.bund.de/index.php/default/digitales-gelandemodell-gitterweite-10-m-dgm10.html (2016).
78. Bryant, S. RFM2019: flood events spatially representative selection. https://doi.org/10.5281/zenodo.13963065 (2024).

79. Bryant, S., Schumann, G., Apel, H., Kreibich, H. & Merz, B. Technical note: resolution enhancement of flood inundation grids. *Hydrol. Earth Syst. Sci.* **28**, 575–588 (2024).
80. BKG. Digitales Geländemodell Gitterweite 5 m. Dataset, https://gdz.bkg.bund.de/index.php/default/digitales-gelandemodell-gitterweite-5-m-dgm5.html (2021).
81. Bryant, S. RFM2019: flood grids downscaled, https://doi.org/10.5281/zenodo.13963132 (2024).
82. Arrighi, C., Pregnolato, M., Dawson, R. J. & Castelli, F. Preparedness against mobility disruption by floods. *Sci. Total Environ.* **654**, 1010–1022 (2019).
83. Zhou, R., Zheng, H., Liu, Y., Xie, G. & Wan, W. Flood impacts on urban road connectivity in southern China. *Sci. Rep.* **12**, 16866 (2022).
84. Schiavina, M., Melchiorri, M., Pesaresi, M., Politis, P. et al. GHSL data package 2023 (GHS P2023), https://publications.jrc.ec.europa.eu/repository/handle/JRC133256 (2023).
85. Wassmer, J. Software: Unveiling hidden risks in healthcare from flood-induced transportation disruption. https://doi.org/10.5281/zenodo.13968711 (2025). Accessed: 2025-08-13.
86. Road Safety Authority. The two-second rule - road safety authority rules of the road. https://web.archive.org/web/20120309213451/http://www.rotr.ie/rules-for-driving/speed-limits/speed-limits_2-second-rule.html (2012).
87. Ecke, L., Chlond, B., Magdolen, M., Vallée, J. & Vortisch, P. Deutsches mobilitätspanel (mop) - wissenschaftliche begleitung und auswertungen. bericht 2020/2021: Alltagsmobilität und fahrleistung. Technical Report, Institut für Verkehrswesen, Karlsruher Institut für Technologie (KIT), Karlsruhe. https://mobilitaetspanel.ifv.kit.edu/downloads/Bericht_MOP_20_21.pdf (2021).
88. Geofabrik GmbH. Openstreetmap data extracts from download.geofabrik.de. Available under the Open Database License (ODbL) 1.0, https://download.geofabrik.de/ (2025).
89. Ecke, L., Chlond, B., Magdolen, M., Vallée, J. & Vortisch, P. Deutsches mobilitätspanel (mop) - wissenschaftliche begleitung und auswertungen bericht 2020/2021: Alltagsmobilität und fahrleistung. Technical Report, Karlsruher Institut für Technologie (KIT) (2021).
90. Bryant, S. Cefect/FloodDownscaler2: V2024-06-29_main. *Zenodo*, https://doi.org/10.5281/zenodo.13963800 (2024).

Acknowledgements

The research presented in this article was conducted within the research training group Natural Hazards and Risks in a Changing World (NatRiskChange) funded by the Deutsche Forschungsgemeinschaft (DFG; GRK 2043/2). We would also like to thank all the members of NatRiskChange for camaraderie and discussions, esp. Karen Lebek and Annegret Thieken for their support and administrative genius. We would also like to thank Heidi Kreibich for her mentorship and supervision. We also thank Viet Dung for his work on RFM and guidance on using and interpreting the results.

Author contributions

J.W. and S.B. jointly conceptualized the study. J.W. contributed the methodology, software, formal traffic analysis and visualization, investigation, data curation and—in tandem with S.B.—project administration. S.B. contributed methodology and software for flood hazard analysis, investigation and data curation and coordinated project tasks. P.S. investigated historical floods and contributed to drafting and revising the manuscript; L.K. also drafted sections and participated in revision. M.P. aided conceptualization and manuscript revision, while J.K. focused on critical review and editing. N.M. and B.M. supplied conceptualization, methodology, resources, funding, supervision and extensive manuscript revision. All authors reviewed and approved the final manuscript.

Funding

Open Access funding enabled and organized by Projekt DEAL.

Competing interests

The authors declare no competing interests.

Additional information

Supplementary information The online version contains supplementary material available at https://doi.org/10.1038/s43247-025-02645-y.

Correspondence and requests for materials should be addressed to Seth Bryant.

Peer review information *Communications Earth & Environment* thanks Elco Koks, Theodore Tsekeris and the other, anonymous, reviewer(s) for their contribution to the peer review of this work. Primary Handling Editors: Kendra Gotangco Gonzales and Martina Grecequet. A peer review file is available